Chapter 14 | Nonhomogeneous Boundary Layers

14.1 Types of Surface Inhomogeneities

Micrometeorological theories, observations, and methods discussed in the preceding chapters are strictly applicable to the atmospheric boundary layer flow over a flat, uniform, and homogeneous terrain. Over such an ideal surface, the PBL is also horizontally homogeneous and in equilibrium with the local surface characteristics, especially when synoptic conditions do not change rapidly. Such a simple state of affairs may exist frequently over open oceans, seas, and large lakes, as well as over extensive desert, ice, snow, prairie, and forest areas of the world. More often, though, land surfaces are characterized by surface inhomogeneities, which make the atmospheric boundary layers over them also nonhomogeneous.

Surface inhomogeneities, which have important effects on atmospheric flows, include boundaries between land and water surfaces (coastlines); the transitions between urban and rural areas or between different types of vegetation; mesoscale oceanic eddies and other regions of varying sea-surface temperature; and hills and valleys. In going over these terrain inhomogeneities, the flow encounters sudden or gradual changes in surface roughness, temperature, wetness, or elevation. Quite often, changes in several surface characteristics occur together, and a complete understanding of modifications in PBL properties (velocity, temperature, and humidity) requires that changes in the surface roughness, temperature, wetness, and elevation be treated simultaneously. For the sake of simplicity and convenience, however, micrometeorologists have studied the effects of changes in the surface roughness, temperature, etc., separately. Due to nonlinearity of the system, however, the individual effects may not simply be additive; the overall effect of a combination of changes in surface characteristics may differ substantially from the sum of individual effects. There are only a few studies of the combined effects of two or more types of surface inhomogeneities occurring simultaneously.

14.2 Step Changes in Surface Roughness

Modification of the boundary layer following a step change in surface roughness normal to the direction of flow has been studied extensively experimentally as well as theoretically. A schematic of the approach flow and the modified flow due to change in the surface roughness is shown in Figure 14.1 for the case of neutral stability. Note that the approach wind profile $U_1(z)$ is a function of the upwind friction velocity u_{*1} and the surface roughness z_{01}. Following the roughness changes from z_{01} to z_{02}, the friction velocity is modified and so is the wind profile near the new surface. Modifications to mean wind profile and turbulence as indicated by computed variances and fluxes are found to be confined to a layer whose thickness increases with distance from the line of discontinuity in the surface. The modified layer is commonly referred to as an internal boundary layer (IBL), because it grows within another boundary layer associated with the approach flow.

Above the IBL, flow characteristics are the same as in the approach flow at the same height above the surface. These are essentially determined by upwind surface characteristics. The influence of the upstream surface may be expected to disappear at a sufficiently large distance from the roughness discontinuity, where the IBL has grown to the equilibrium PBL depth for the new surface, or it is otherwise limited by a strong low-level inversion.

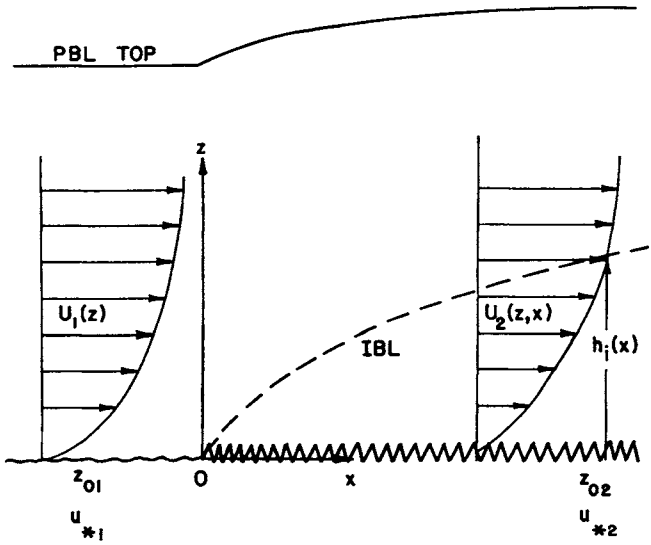

Figure 14.1 Schematic of the internal boundary layer development and wind-profile modification following a step change in the surface roughness.

In some of the earliest experimental studies of flow over a step change in surface roughness, hundreds of bushel baskets or Christmas trees were placed on a frozen lake (Lake Mendota, Wisconsin) in winter and modifications to the near-surface wind and temperature profiles due to the change in roughness were studied (Kutzback, 1961; Stearns and Lettau, 1963). The observed wind profiles did not extend beyond a height of 3.2 m and no independent shear stress or drag measurements were made in these experiments.

A more comprehensive field study was conducted by Bradley (1968), who measured changes in the surface shear stress and wind profiles with distance from the roughness discontinuity in going from a comparatively 'smooth' (but aerodynamically rough) tarmac surface (z_0 = 0.02 mm) to a moderately rough surface of wire mesh with spikes (z_0 = 2.5 mm), and vice versa. Figure 14.2

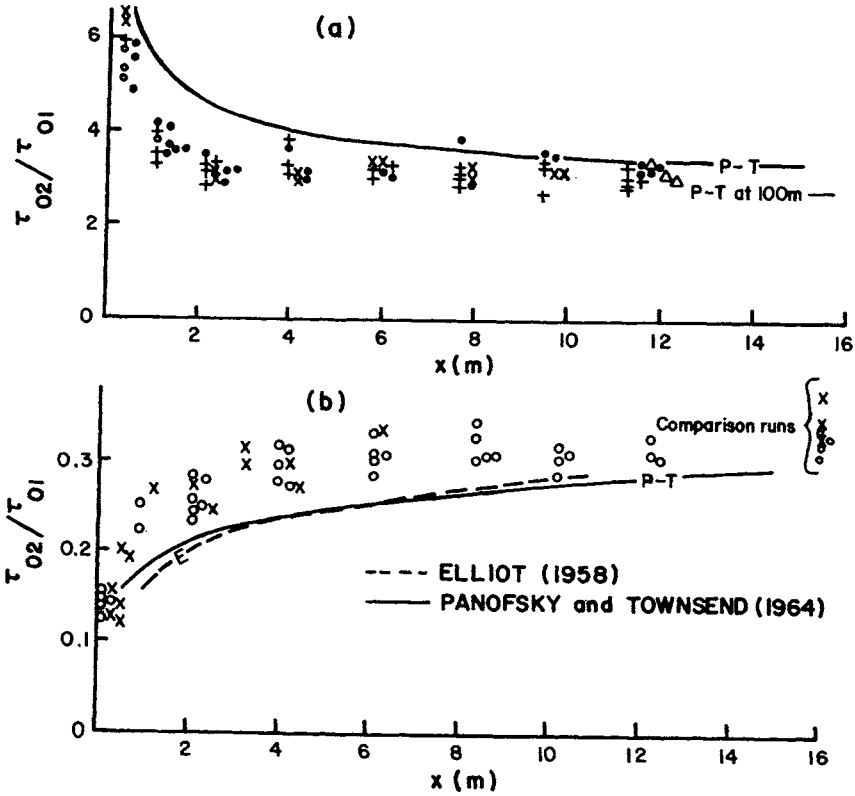

Figure 14.2 Observed variations of the normalized surface shear stress downwind of (a) smooth to rough (from z_0 = 0.02 mm to z_0 = 2.5 mm) and (b) rough to smooth (from z_0 = 2.5 mm to z_0 = 0.02 mm) transitions compared with certain theories. [After Bradley (1968).]

shows the variations in surface stress with distance for the two cases (smooth to rough and rough to smooth) of the internal boundary layer flow under near-neutral stability conditions. Here the local stress is normalized by the magnitude of the equilibrium stress for the upwind surface.

Note that the observations of Figure 14.2 indicate that there is a rather sharp change in the surface stress near the roughness discontinuity, with a considerable amount of overshoot above or undershoot below its expected equilibrium value for the new (rougher or smoother) surface. Relaxation to the equilibrium value occurs very rapidly in the first few meters and gradually thereafter. No detectable changes in the surface stress are apparent from observations beyond a distance of 10–15 m from the roughness discontinuity. But a number of theoretical and numerical model studies predict slow adjustment occurring over much longer distances (Elliot, 1958; Panofsky and Townsend, 1964; Rao *et al.*, 1974); some of these theoretical results are shown in Figure 14.2.

Observed changes in the wind profile following step changes in the surface roughness from smooth to rough and vice versa, are shown in Figure 14.3. At any downwind distance from the surface discontinuity, the lower part of the wind profile is representative of the local surface, while the upper part represents the upwind surface.

Within the lowest 10–15% of the PBL the velocity profile in neutral stability may be approximated as (Elliot, 1958)

$$\begin{aligned} U &= (u_{*2}/k)\ln(z/z_{02}), \quad \text{for } z \le h_i \\ U &= (u_{*1}/k)\ln(z/z_{01}), \quad \text{for } z > h_i \end{aligned} \tag{14.1}$$

In reality, the IBL is not as sharply defined as is implied by the discontinuity (kink) in the velocity profile [Equation (14.1)], and there is a finite blending region around $z = h_i$ in which the velocity profile gradually changes from one form to another. There is also a question about the validity of the log law in the lower layer, especially in the region where the friction velocity might be changing rapidly and has not reached its equilibrium value u_{*2}. The more appropriate equations of mean motion in the lower part of the IBL, where the Coriolis effects can be neglected, are

$$\begin{aligned} U(\partial U/\partial x) + W(\partial U/\partial z) &= \partial \tau_{zx}/\partial z \\ \partial U/\partial x + \partial W/\partial z &= 0 \end{aligned} \tag{14.2}$$

which form the basis for simpler theoretical models. Note that eliminating the pressure gradient and Coriolis acceleration terms from Equation (14.2) would limit their validity to rather short distances from the surface discontinuity.

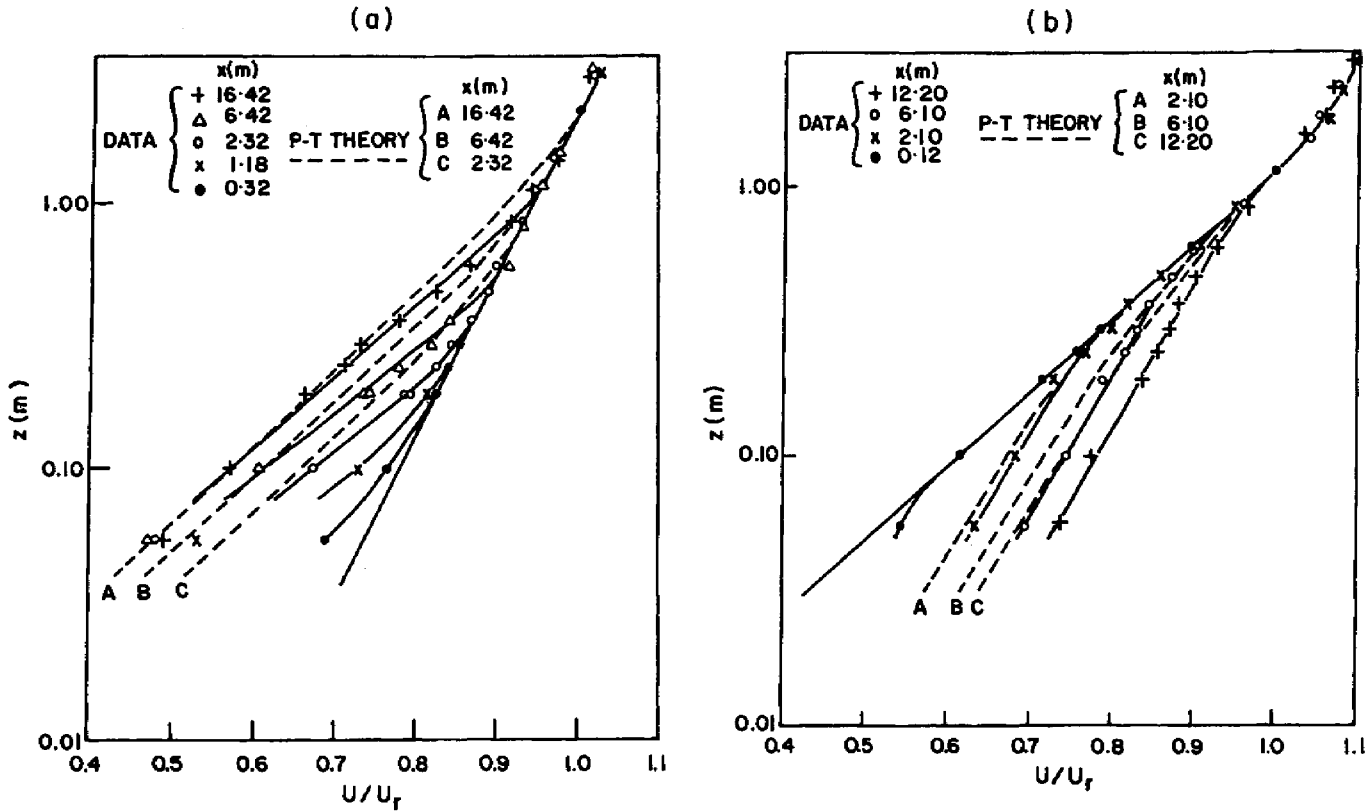

Figure 14.3 Observed modifications of mean velocity profiles downwind of (a) smooth to rough (from $z_0 = 0.02$ mm to $z_0 = 2.5$ mm) and (b) rough to smooth (from $z_0 = 2.5$ mm to $z_0 = 0.02$ mm) transitions compared with Panofsky and Townsend's (1964) theory. [After Bradley (1968).]

According to a number of field and laboratory observations taken under neutral stability conditions, the growth of the internal boundary layer thickness follows an approximate power law

$$h_i/z_{02} = a_i(x/z_{02})^{0.8} \tag{14.3}$$

with estimated values of the empirical constant a_i between 0.35 and 0.75. Actually, a_i depends also on the definition of the IBL thickness. The top of the IBL may be defined as the level where mean wind speed, turbulent momentum flux, or one of the velocity variances reaches a specified fraction (0.90–0.99) of its upstream equilibrium value. An experimental verification of Equation (14.3) is shown in Figure 14.4, using Bradley's (1968) field data and those from a wind tunnel simulation. Interestingly, the value of the exponent in Equation (14.3) is the same as that in the approximate classical relationship for the growth of a turbulent boundary layer over a flat plate parallel to the flow (Schlichting, 1960).

More recent modeling studies of the mean flow and turbulence structure in a neutral boundary layer over a change in surface roughness have also indicated small modifications in the flow upstream of the roughness change or discontinuity (Claussen, 1987). The models based on the TKE closure are found to give much better agreement with experimental data than those based on the first-order (eddy viscosity or mixing length) closure (Claussen, 1988).

Effects of stability on the development of internal boundary layers over warmer and colder than air surfaces have not been investigated systematically. A few experimental and theoretical studies of the IBL under unstable conditions suggest that Equation (14.3) may also be applicable to these conditions, perhaps with a larger value of a_i than for the neutral case. The IBL growth in a stably stratified atmosphere, on the other hand, may be expected to be slower, suggesting smaller values of the coefficient a_i and possibly also of the exponent in Equation (14.3). There is a definite need for further studies of the growth and structure of the IBL under stably stratified conditions.

There have been a few experimental and theoretical studies of the wind-profile modification and the IBL development to large distances of the order of tens of kilometers from the roughness discontinuity, where the Coriolis effects cannot be ignored. It is found that there is a gradual shifting of surface wind direction in a cyclonic or anticyclonic sense in going from smooth to rough or rough to smooth surface, respectively. For example, wind direction shifts of 10–20° have been observed in air flowing from rural to urban areas and vice versa (Oke, 1974). Such changes in the surface wind direction can be explained in terms of the observed dependence of the surface cross-isobar angle (α_0) on surface roughness (α_0 increases with surface roughness, as discussed in Chapter 6). These wind direction changes have important implications for plume trajectories crossing urban and rural boundaries, as well as shorelines. They

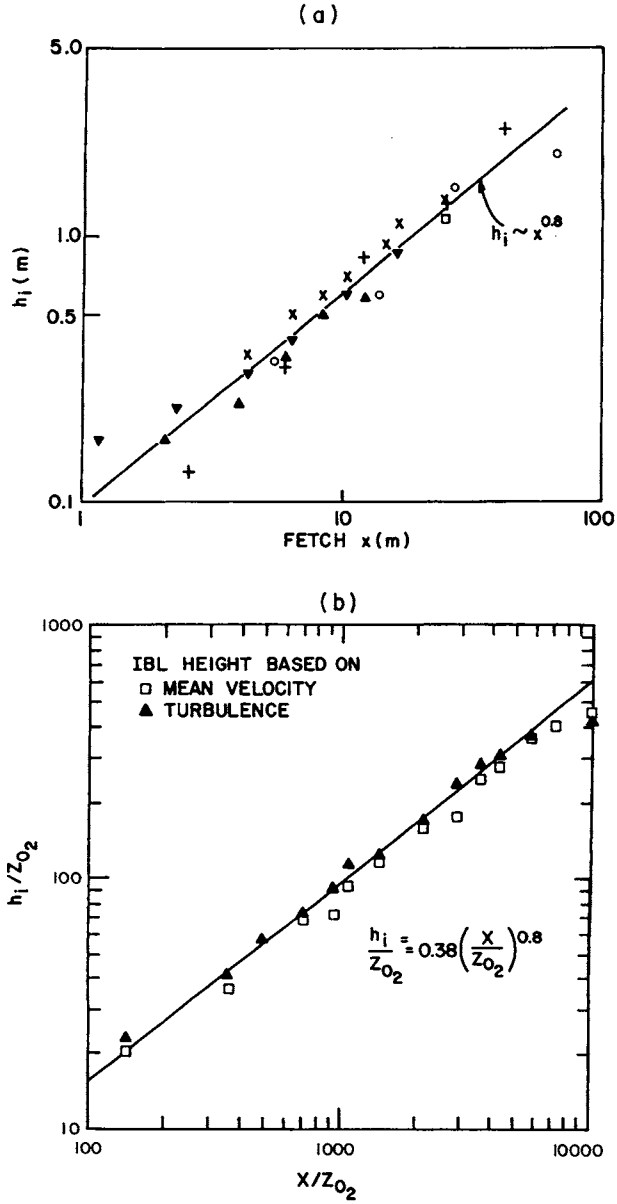

Figure 14.4 Observed thickness of the internal boundary layer as a function of distance downwind of a step change in the surface roughness based on (a) Bradley's (1968) field data and (b) Pendergrass and Arya's (1984) wind tunnel data. [(b) Reprinted with permission from *Atmospheric Environment*, Copyright © (1984), Pergamon Journals Ltd.]

may also result in distribution of horizontal divergence and convergence and associated distributions of clouds and precipitation.

Many natural surfaces actually present a series of step changes in surface roughness corresponding to different land uses. In principle, one can think of an IBL associated with each step change in surface roughness, so that after a few steps the PBL would be composed of several IBLs. The wind profile is not simply related to the local roughness, except in a shallow surface layer, but represents the integrated effects of several upwind surfaces, depending on the layer (height range) of interest. Observed wind profiles under such conditions often show kinks (discontinuities in slope) when U is plotted against log z; each kink may be associated with an interface between the adjacent IBLs. Such a fine tuning of the wind profile and identification of IBL interfaces may not be possible, however, unless the wind profile is adequately averaged, well resolved, and taken under strictly neutral conditions (most routine wind soundings do not meet these requirements).

14.3 Step Changes in Surface Temperature

Differences in albedos, emissivities, and other thermal properties of natural surfaces lead to their different surface temperatures, even under a fixed synoptic weather setting. Consequently, inhomogeneities in surface temperature may occur independently of changes in surface roughness. Most dramatic changes in surface temperature occur across lake shorelines and sea coastlines. In response to these abrupt changes in surface characteristics, thermal internal boundary layers develop over land during onshore flows and over water during offshore flows. Thermal boundary layers also develop in air flow from rural to urban areas and vice versa. On still smaller scales, thermal internal boundary layers develop near the boundaries of different crops, as well as across roads and rivers (Rider *et al.*, 1963).

When temperature differences between two or more adjacent surfaces are large enough and the ambient (geostrophic) flow is weak, thermally induced local or mesoscale circulations are likely to develop on both sides of surface temperature discontinuity. The best known examples of such circulations are the land and sea breezes. Internal boundary layers are often embedded in such thermally driven mesoscale circulations.

14.3.1 Thermal IBL growing over a warmer surface

Perhaps the most dramatic changes in the atmospheric boundary layer occur when stably stratified air flowing over a cold surface encounters a much warmer

(relative to air) surface. This frequently occurs in coastal areas during midday and afternoon periods; the resulting flow is called a sea breeze or lake breeze. A similar situation on a large scale occurs during periods of cold-air outbreaks over relatively warm waters (e.g., Great Lakes, Gulf Stream, and Kuroshio) in late fall or winter.

If the temperature difference between downwind and upwind surfaces is fairly large (say, $\Theta_{02} - \Theta_{01} > 5$ K), the thermal internal boundary layer (TIBL) developing over the warmer surface would most likely be very unstable or convective (Figure 14.5). The growth of such a TIBL can be described by a simple mixed-layer model based on the mean thermodynamic energy equation, under stationary conditions

$$U(\partial\Theta/\partial x) = -(1/\rho c_p)(\partial H/\partial z) \tag{14.4}$$

Integrating Equation (14.4) with respect to z from 0 to h_i gives

$$h_i U_m(\partial\Theta_m/\partial x) = (1/\rho c_p)(H_0 - H_i) \tag{14.5}$$

in which U_m and Θ_m are the mixed-layer averaged wind speed and potential temperature and H_0 and H_i are the heat fluxes at the surface and at the top of the TIBL or mixed layer ($z = h_i$), respectively. An equation for the growth of the TIBL with distance x from the temperature discontinuity can be obtained after making reasonable assumptions about the potential temperature profile and the heat flux profile, as shown in Figure 14.5. From these it is clear that

$$\begin{aligned} \Theta_m &= \Theta_{01} + \gamma h_i - \Delta\Theta \\ \partial\Theta_m/\partial x &= \gamma(\partial h_i/\partial x) \end{aligned} \tag{14.6}$$

where $\gamma \equiv (\partial\Theta/\partial z)_0$ is the potential temperature gradient in the approach flow, which is also the gradient above the TIBL. Here, we have assumed that the jump in potential temperature ($\Delta\Theta$) at the top of the TIBL remains constant. If one also assumes that the downward heat flux at the top of the TIBL is a constant fraction of the surface heat flux, i.e., $H_i = -AH_0$, Equations (14.5) and (14.6) yield an expression for the height of the TIBL

$$h_i = a_1(H_0 x/\rho c_p U_m \gamma)^{1/2} \tag{14.7}$$

in which $a_1 = (2 + 2A)^{1/2} \cong 1.5$ is an empirical constant. The use of Equation (14.7) requires the knowledge of the surface heat flux and the mixed-layer wind speed over the downwind heated surface, in addition to that of γ.

An alternative, simpler formula is obtained by expressing or parameterizing the surface heat flux as $H_0 = \alpha\rho c_p U_m(\Theta_{02} - \Theta_{01})$, where $\alpha \cong 2.1 \times 10^{-3}$ is an

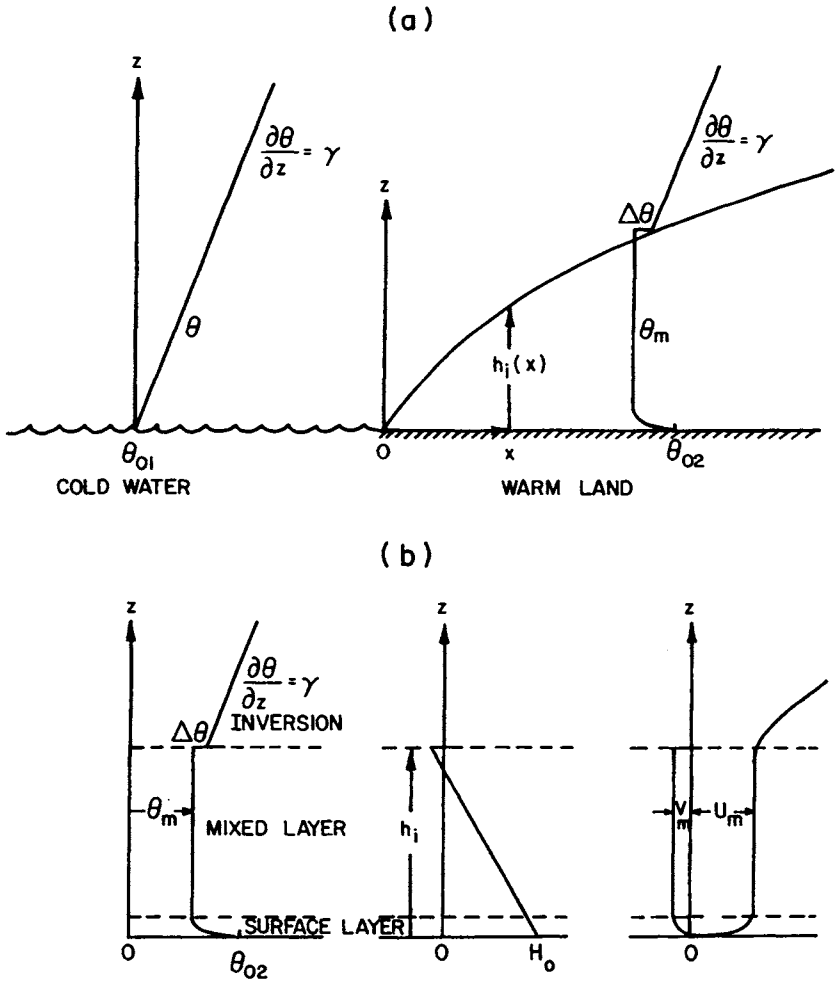

Figure 14.5 (a) Schematic of a thermal internal boundary layer developing when a stable air flow encounters a much warmer surface, and (b) idealized potential temperature, heat flux, and wind profiles in the same.

empirical coefficient (Vugts and Businger, 1977). Then, Equation (14.7) can be expressed as

$$h_i = a_2[(\Theta_{02} - \Theta_{01})x/\gamma]^{1/2} \tag{14.8}$$

where $a_2 = [2(1 + A)\alpha]^{1/2} \cong 0.1$. This does not require the knowledge of surface heat flux or mixed-layer wind speed. The latter is introduced in the TIBL height

expression if one uses the more conventional bulk transfer formula for the surface heat flux

$$H_0 = C_H \rho c_p U_m (\Theta_{02} - \Theta_m)$$

with $C_H \approx C_D = (u_*/U_m)^2$. This type of parameterization leads to the TIBL height formula

$$h_i = a_3 (u_*/U_m)[(\Theta_{02} - \Theta_m)x/\gamma]^{1/2} \tag{14.9}$$

with $a_3 \cong [2(1 + A)C_H/C_D]^{1/2} \cong 2.0$. The above expression has the disadvantage of containing the x-dependent variables U_m and Θ_m of the modified mixed layer. Implicit or explicit relations for the variation of Θ_m with x have been given (Fleagle and Businger, 1980). Using some additional assumptions, the TIBL height can also be expressed as (Venkatram, 1977)

$$h_i = a_4 (u_*/U_m)[(\Theta_{02} - \Theta_{01})x/\gamma]^{1/2} \tag{14.10}$$

where $a_4 \cong 1.7$. Some of the above expressions for h_i have been compared and verified against observations (Raynor *et al.*, 1979; Stunder and SethuRaman, 1985). Equation (14.7) appears to be the best, because its derivation involves the least number of assumptions.

The above-mentioned formulations of the TIBL growth are based on mixed-layer assumptions for the TIBL and neglect of the near-surface layer, in which velocity and potential temperature generally have strong gradients. These are not expected to be valid for short (less than 1 km) distances from the temperature discontinuity, where modifications are likely to be confined to the shallow surface layer. Detailed experimental investigations of air modification in the surface layer in the immediate vicinity of a step change in surface temperature have been reported by Rider *et al.* (1963) and Vugts and Businger (1977). Here, the growth of the TIBL is more rapid and more closely follows the $x^{0.8}$ behavior, similar to that of an IBL following a step change in roughness (Elliot, 1958). Turbulent characteristics of a shallow convective internal boundary layer have been studied by Smedman and Hogstrom (1983).

A number of experimental and numerical modeling studies have been conducted on large lake/sea breezes and thermal internal boundary layers associated with such breezes (Pielke, 1984; Arritt, 1987). It is found that water surface temperature has little effect on lake breeze development, as long as the water is cold enough that the boundary layer over the lake is stably stratified. If the lake surface is warmer than air, the more vigorous fluxes due to convective turbulence produce major changes in the lake breeze (Arritt, 1987). Lake and sea breezes are more commonly observed during late spring and summer

seasons when land surface gets rapidly heated up during mid-day and afternoon hours.

14.3.2 Thermal IBL growing over a colder surface

As compared to the rapidly growing and highly energetic unstable or convective TIBL developing in cold air advecting over a much warmer surface, the reverse situation of comparatively shallow and smooth stable TIBL that develops in warm air advection over a colder surface has received very little attention. An early observational study was made by Taylor (1915) on the ice-scout ship SS Scotia near the coast of Newfoundland. More recently, Raynor *et al.* (1975) have reported on some measurements of the depth of the stable TIBL at the southern shore of Long Island, New York, as a function of fetch. The TIBL resulted from modification of warm continental air following a southwesterly trajectory over colder oceanic waters; its depth could be represented by an empirical relationship

$$h_i = a_5(u_*/U)[(\Theta_{01} - \Theta_{02})x/|\partial T/\partial z|]^{1/2} \tag{14.11}$$

which is similar to Equation (14.10) for the unstable TIBL. Here, $|\partial T/\partial z|$ is the absolute value of the lapse rate or temperature gradient over the source region or above the inversion in the modified air, U is the mean wind speed at a reference level (say, 10 m) near the surface, and a_5 is an empirical constant of the order of unity which may depend on the choice of the reference level for measuring or specifying wind speed.

Note that despite the apparent similarities of the TIBL height equations [Equations (14.10) and (14.11)] in different situations of cold- and warm-air advection, respectively, for a given fetch the magnitudes of h_i and $\partial h_i/\partial x$ are found to be much smaller in the latter case. These and other IBL height equations showing unrestricted growth of internal boundary layers with fetch or distance from the discontinuity in the surface roughness, temperature, etc., must cease to be valid beyond a certain distance where the IBL has grown to the equilibrium depth of the PBL for the given surface and external conditions. Observations indicate that this might take tens to hundreds of kilometers, depending on the equilibrium PBL depth.

Example Problem 1

Calculate and compare the development of thermal internal boundary layers in the following two different situations:

(a) A stably stratified boundary-layer flow with $\partial\Theta/\partial z = 0.05$ K m^{-1} overland advecting over a 10°C warmer sea.

(b) An unstable continental boundary-layer flow with an average lapse rate of $0.015\ \text{K m}^{-1}$ in the surface layer advecting over a 10°C colder sea surface. Assume a typical value of $C_D = 0.5 \times 10^{-3}$ for the stably stratified TIBL.

Solution

(a) The appropriate expression for the TIBL height in this case is Equation (14.8)

$$h_i = a_2[(\Theta_{02} - \Theta_{01})x/\gamma]^{1/2}$$

in which $\Theta_{02} - \Theta_{01} = 10$ K, $\gamma = 0.05\ \text{K m}^{-1}$, and $a_2 \cong 0.1$.
Substituting these values in the above expression, we get

$$h_i \cong 1.414x^{1/2}$$

in which x is in meters. The computed TIBL heights at various distances offshore are:

x (m):	100	200	500	1000	2000	5000	10 000	20 000
h_i (m):	14.1	20.0	31.6	44.7	63.2	100	141	200

(b) The appropriate expression for the TIBL height growing over the colder sea surface is Equation (14.11)

$$h_i = a_5 \frac{u_*}{U}\left[\frac{(\Theta_{01} - \Theta_{02})x}{|\partial T/\partial z|}\right]^{1/2}$$

where, $a_5 \cong 1.0$, $u_*/U = C_D^{1/2} = 0.02236$, $\Theta_{01} - \Theta_{02} = 10$ K, and $\partial T/\partial z = -0.015\ \text{K m}^{-1}$.
Substituting these values in the above expression, we obtain

$$h_i \cong 0.577x^{1/2}$$

in which x is in meters. The computed heights of the stable TIBL at various distances offshore are:

x (m):	100	200	500	1000	2000	5000	10 000	20 000
h_i (m):	5.7	8.2	12.9	18.2	25.8	40.8	57.7	81.6

Note that the stable TIBL growing over the colder sea surface is much shallower than the unstable TIBL growing over the warmer sea.

14.4 Air Modifications over Water Surfaces

When continental air flows over large bodies of water, such as large lakes, bays, sounds, seas, and oceans, it usually encounters dramatic changes in surface roughness and temperature. Consequently, significant modifications in air temperature, specific humidity, cloudiness, winds, and turbulence occur in the developing IBLs with distance from the shoreline. Most dramatic changes in air properties and ensuing weather phenomena occur when cold air flows over a much warmer water surface. Intense heat and water vapor exchanges between the water surface and the atmosphere lead to vigorous convection, formation of clouds, and, sometimes, precipitation. Some examples of this phenomenon are frequent cold-air outbreaks over the warmer Great Lakes in late fall and early winter and the resulting precipitation (often, heavy snow) over immediate downwind locations. It has been the focus of several field experiments, including the 1972 International Field Year of the Great Lakes (IFYGL). Figure 14.6 presents the observed changes in potential temperature and cloudiness across Lake Michigan during a cold-air outbreak when the water–air temperature difference was about 12.5 K (Lenschow, 1973). Note the rapid warming and

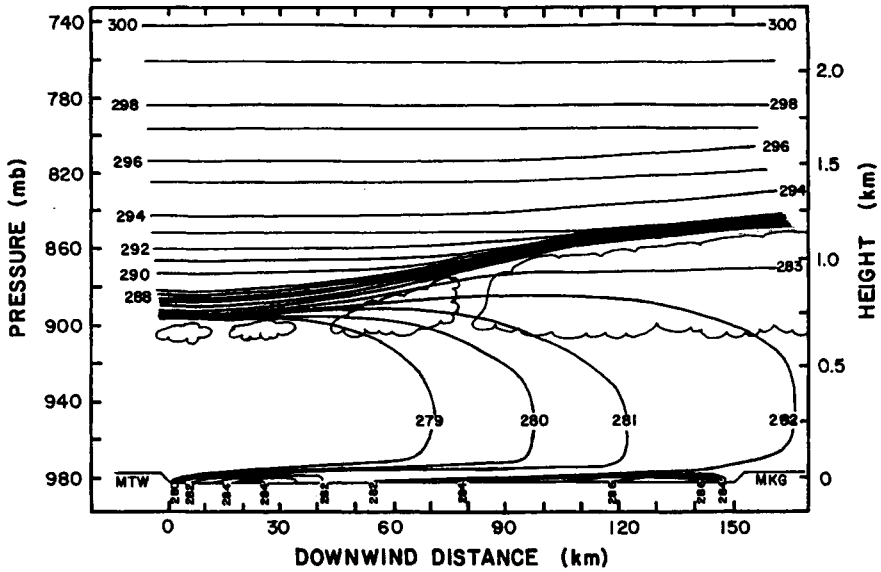

Figure 14.6 Observed modifications in potentials temperature and cloudiness across Lake Michigan during a cold-air outbreak on November 5, 1970. Mean wind is from left to right. [After Lenschow (1973).]

moistening of the approaching cold, dry air mass by the warmer lake surface water.

Other major investigations of air modification during cold-air outbreaks over warm waters have been conducted during the 1974 and 1975 Air Mass Transformation Experiments (AMTEX) over the Sea of Japan and a more recent (1986) Genesis of Atlantic Lows Experiment (GALE). In the latter experiment was observed one of the most intense cold-air outbreaks with air–sea temperature differences of 20–25 K over the Gulf Stream just off the North Carolina coast. The ocean-surface temperature here varies considerably with distance from the coast, with several step changes between the coast and the eastern edge of the Gulf Stream. Several research aircraft, ships, and buoys were used to study air-mass modifications in the boundary layer at different locations. The cold-air outbreak of January 28, 1986, was most spectacular in that the ocean surface was enshrouded in a steamlike fog with abundant number of steam devils, water spouts, and other vortexlike filaments visible from low-flying aircraft. The PBL depth increased from about 900 m at 35 km offshore to 2300 m at the eastern edge of the Gulf Stream (284 km offshore). At the same time, the cloudiness increased from zero to a completely overcast, thick deck of stratocumulus with snow and rainshowers developing over the eastern edge of the Gulf Stream. The subcloud mixed layer was characterized by intense convective turbulence with strong updrafts and downdrafts (Wayland and Raman, 1989).

A simple theory of predicting changes in air temperature and specific humidity as a function of fetch for the case of cold-air advection over a warm sea, but in the absence of condensation and precipitation processes in the modified layer, is given by Fleagle and Businger (1980). When the top of the TIBL reaches above the lifting condensation level, however, the structure of the TIBL changes dramatically. Complex interactions take place between cloud particles, radiation, and entrainment at the top of the TIBL. These and complex topographical effects can be considered in numerical mesoscale PBL models (Huang and Raman, 1990).

Modifications of warm continental air advecting over a cold lake or sea surface are equally dramatic, but the modified layer is much shallower. Turbulence is considerably reduced in this shallow, stably stratified TIBL, while visibility may be reduced due to fog formation under appropriate conditions. Cases of strong warm-air advection commonly occur in springtime over the Great Lakes and along the east coast of the United States and Canada. Figure 14.7 presents some observations of air modification under such conditions prevailing over Lake Michigan (Wylie and Young, 1979). These were made from a ship traveling in the downwind direction across the lake, with instruments attached to a tethered balloon. Note that the surface-based inversion that formed over water rose to about 140 m after a fetch of 50 km

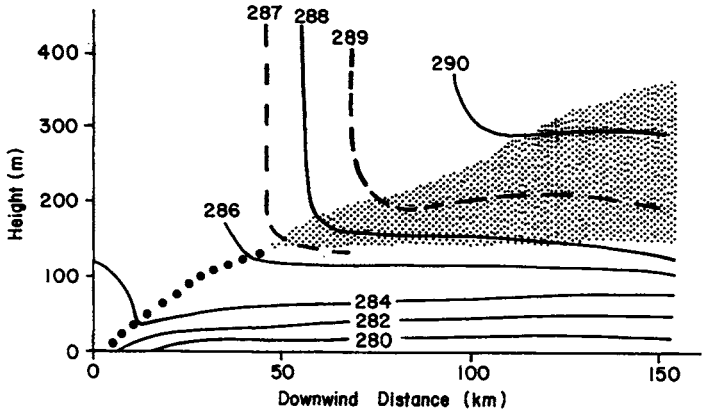

Figure 14.7 Observed modifications in potential temperature over Lake Michigan during warm-air advection. Surface-based inversion is unshaded area below the dotted line; shading denotes stable isothermal layer. [After Wylie and Young (1979). Copyright © (1979) by D. Reidel Publishing Company. Reprinted by permission.]

and remained at a constant level for the rest of the fetch along the lake. A growing isothermal layer separated the surface inversion layer from the adiabatic mixed layer advected from upwind land areas. Large variations in wind speed and direction were observed within the inversion layer. Note that the thermal internal boundary layer, including the isothermal layer, kept growing over the whole fetch of more than 150 km across the lake.

14.5 Air Modifications over Urban Areas

Urbanization, which includes residential, commercial, and industrial developments, produces radical changes in radiative, thermodynamic, and aerodynamic characteristics of the surface from those of the surrounding rural areas. Therefore, it is not surprising that as urbanization proceeds the associated weather and climate often are modified substantially. Such modifications are largely confined to the so-called urban boundary layer, although the urban 'plume' of pollutants originating from the city may extend hundreds of kilometers downwind. Many studies of urban influences have identified significant changes in surface and air temperatures, humidity, precipitation, fog, visibility, air quality, surface energy fluxes, mixed-layer height, boundary layer winds, and turbulence between the urban and rural areas. Here, we give a brief description of some of the better known urban-induced phenomena.

14.5.1 The urban heat island

The most frequently observed (or felt) and best documented climatic effect of urbanization is the increase in surface and air temperatures over the urban area, as compared to rural surroundings. Closed isotherms over the urban and suburban areas generally separate these areas from the rural environs. This condition or phenomenon has come to be known as the urban heat island, because of the apparent similarity of isotherms to contours of elevation for a small, isolated island in the ocean. This analogy is carried further in the schematic representation of near-surface temperature in Figure 14.8 for a large city on a clear and calm evening, as one travels from the countryside to the city center. This shows a typical 'cliff' of steep rise in temperature near the rural/suburban boundary, following by a 'plateau' over much of the suburban area, and then a 'peak' over the city center (Oke, 1987, 1995). The maximum difference in the urban peak temperature and the background rural temperature defines the urban heat-island intensity (ΔT_{u-r}). Over large metropolitan areas, there may be several plateaus and peaks in the surface temperature trace. Also, there are likely to be many small-scale variations in response to distinct intraurban land uses, such as parks, recreation areas, and commercial and industrial developments, as well as topographical features, such as lakes, rivers, and hills. Strictly urban influences on the local weather and climate can be studied in an isolated manner only in certain interior (as opposed to coastal) cities in relatively flat terrain. For this reason, St Louis, Missouri, was chosen to be the arena for several large field studies, viz., Metropolitan Meteorological Experiment (METROMEX, 1971–1976) and Regional Air Pollution Study (RAPS, 1973–1977), of urban influences on local weather and climate.

Figure 14.9 shows a map of the St Louis metropolitan area representing major land-use types. The principal urban area is located about 16 km south of the confluence of the Mississippi and Missouri rivers. The primary topographic

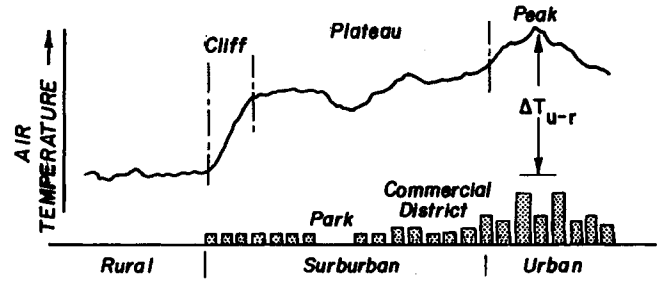

Figure 14.8 Schematic representation of variation in air temperature in going from a rural to an urban area. [After Oke (1987).]

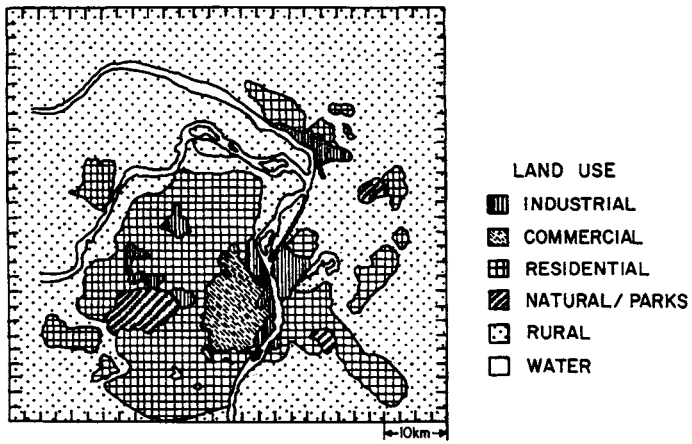

Figure 14.9 Land use map of the Saint Louis Metropolitan area during RAPS. [After Byun (1987).]

features in the area are the river valley with a prominent bluff rising 20–60 m above the flood plain east of the merged river and heavily wooded (70–90 m in height) hills to the southwest. A slightly smoothed pattern of aircraft-observed (with an infrared radiometer) ground-surface temperatures on a clear, summer afternoon is shown in Figure 14.10. Note that it clearly shows the urban heat-island phenomenon with an intensity of $\Delta T_{u-r} \cong 8.4$ K at that particular time. The difference in air temperatures at a 10 m height is likely to be much smaller.

Other observations of the urban heat island over small and large cities have been reviewed by Landsberg (1981) and Oke (1974, 1995). The intensity of an urban heat island depends on many factors, such as the size of city and its energy consumption, geographical location, month or season, time of day, and synoptic weather conditions. The maximum intensity for a given city occurs in clear and calm conditions (e.g., under a stationary high), a few hours after sunset. The intensity becomes minimal or zero under highly disturbed (stormy), windy weather conditions.

Under reasonably stationary synoptic weather conditions, the heat-island intensity shows a pronounced diurnal variation with a minimum value around midday and maximum value around or before midnight (Oke, 1987, Chapter 8). There are likely to be marked differences in the diurnal variations of ΔT_{u-r} between winter and summer related to the anthropogenic heat release.

Some attempts have been made to correlate the maximum nocturnal heat-island intensity (based on air temperatures at 10 m above ground level) with population (considered as a surrogate for the city size and energy consumption) and near-surface wind speed. Figure 14.11 shows different relationships of

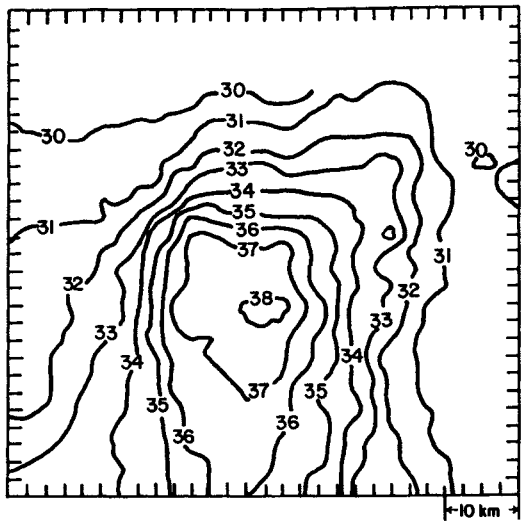

Figure 14.10 Observed patterns of ground-surface temperatures showing the heat-island phenomenon over the Saint Louis Metropolitan area during RAPS. [After Byun (1987).]

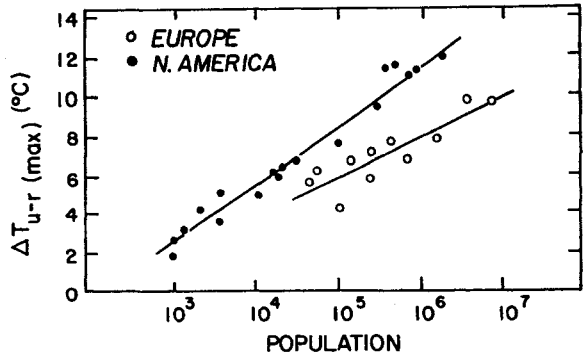

Figure 14.11 Empirical relation between the observed heat-island intensity and city population for North American and European cities. [After Oke (1987).]

$\Delta T_{(u-r)max}$ with population (P) for some of the cities of Europe and North America with minimal topographical influences. Different curves probably reflect differences in the per capita energy consumption and in population density between European and North American cities. The data and regression lines in Figure 14.11 are for calm and cloudless conditions. For moderate wind speeds, ΔT_{u-r} is found to decrease in inverse proportion to the square root of regional (nonurban) wind speed, and vanishes at a 'critical' wind speed of about

9 m s^{-1} (measured at a height of 10 m at a rural site) for large cities (Oke, 1987, Chapter 8).

The use of city population alone is not very satisfactory in explaining the maximum intensity of urban heat island. A much stronger correlation and apparently unique relationship is obtained between the maximum heat-island intensity and the geometry of the street canyons in the city center, as characterized by the average height to width (H/W) ratio. The following regression relationship has been obtained from the data from 31 cities in North America, Europe, and Australia (Oke, 1987, Chapter 8):

$$\Delta T_{u-r(max)} = 7.54 + 3.97 \ln(H/W) \tag{14.12}$$

This relationship indicates that urban canyon geometry exerts a fundamental control on the urban heat island. Urban geometry and the density of development influence physical processes such as the trapping of both incoming solar and outgoing longwave radiations, the amount of anthropogenic heat released in the urban area, and turbulent transports within urban canyons.

The extent and intensity of the urban heat island is also greatly influenced by topography and the presence of large bodies of water within or around the urban area. In coastal cities, land and sea breezes have a profound influence, while in hilly areas nocturnal drainage and valley flows may dominate over the strictly urban influences.

What are the causes for the urban heat-island phenomenon? A number of causes have been hypothesized and most of them are verified by observations. The leading candidates are (Oke, 1987, Chapter 8) as follows:

- Increased incoming longwave radiation ($R_{L\downarrow}$) due to absorption of outgoing longwave radiation and re-emission by polluted urban atmosphere.
- Decreased outgoing longwave radiation loss ($R_{L\uparrow}$) from street canyons due to a reduction in their sky view factor by buildings.
- Increased shortwave radiation (R_S) absorption by the urban canopy due to the effect of street canyons on albedo.
- Greater daytime heat storage (ΔH_s) due to the thermal properties of urban materials and heat release at nighttime.
- Addition of anthropogenic heat (H_a) in the urban area in process emission (heating and cooling), transportation, and industrial operations.
- Decreased evaporation and, hence, the latent heat flux (H_L) due to the removal of vegetation and surface waterproofing of the city.

In short, all the components of the energy balance in the urban canopy are modified in such a way that they add to the heat-island effect in the positive sense. Some of these are effective only during daytime when they contribute to

the storage of heat in the urban canopy; heat release at nighttime keeps the urban air warmer. The relative role of each component is likely to differ from one season to another and also from one city to another.

14.5.2 The urban boundary layer

The urban boundary layer (UBL) is modified by both the urban heat island and the increased roughness (one can also think of an urban area as a 'roughness island'). In the absence of any topography, the roughness elements of a city are its buildings, whose heights (h_0) generally increase toward the city center. Practical considerations make it difficult to determine the value of the roughness length or parameter (z_0) directly from wind-profile measurements over a large city center or commercial area; such observations should be made above the prevailing height of the buildings. But rough estimates can be made by extrapolating the z_0/h_0 and d_0/h_0 relationships discussed in Chapter 10 (as in the case of tall vegetation, the roughness parameterization of an urban canopy must include a zero-plane displacement). In an urban area, the roughness parameter may vary from fractions of a meter in suburbs to several meters over the city center (Grimmond and Oke, 1999).

In near-calm or weak-wind and clear-sky conditions, thermal modification of the boundary layer in response to the urban heat island is likely to dominate over increased roughness effects. The thermally induced circulation that is superimposed on any weak background flow is radially inward toward the city center at lower levels and outward from the city center at upper levels, with a rising motion over the center and subsidence over the surrounding environs. During the day this circulation may extend up to the base of the lowest inversion, which may then acquire a dome shape in response to the induced circulation (rising and subsiding motions). Since mixing is likely to be restricted to the mixed layer below the inversion, it is also referred to as the 'mixed-layer dome,' or 'dust dome,' in which dust, smoke, and haze from urban emissions accumulate during stagnant conditions. Figure 14.12 depicts a schematic of thermally induced circulation and dust dome over an urban area. Figure 14.13 shows the same (mixed-layer dome) with aircraft-observed profiles of potential temperature and specific humidity in the UBL of St Louis, Missouri (Spangler and Dirks, 1974). At that time, winds were nearly uniform in the lowest 500 m, variable above this height up to the inversion base, and again uniform at 5 m s^{-1} above the inversion. Note that a rural-to-urban variation in mixed-layer height of at least 400 m was observed even when the urban heat-island intensity was not particularly strong ($\Delta T_{u-r} < 1$ K).

Aircraft measurements of turbulent fluxes and variances in the daytime UBL also indicate considerable urban-scale variations of these parameters (Ching,

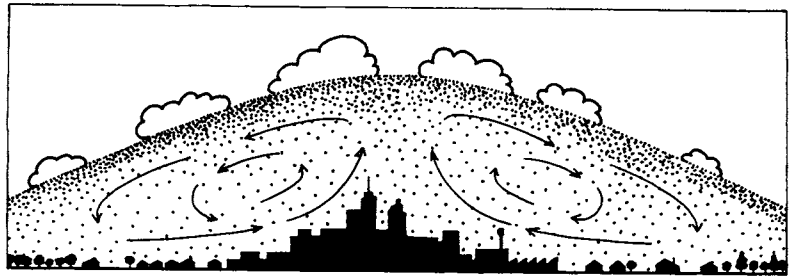

Figure 14.12 Schematic of dust dome and thermally induced circulations over a large city under calm or light winds. [After Lowry (1967). Copyright © (1967) by Scientific American, Inc. All rights reserved.]

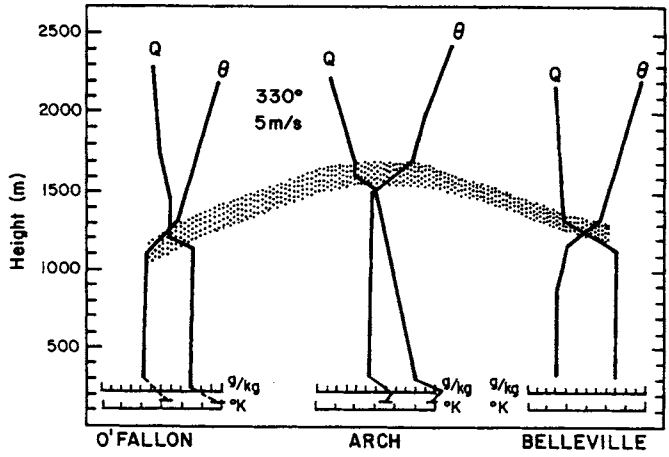

Figure 14.13 Observed mixed-layer dome and potential temperature and specific humidity profiles over Saint Louis on 12 August 1971. [After Spangler and Dirks (1974). Copyright © (1974) by D. Reidel Publishing Company. Reprinted by permission.]

1985). For example, observations over St Louis show that the sensible heat flux varied by a factor of 2 to 4, with the largest values over the city center. The latent heat flux also varied by a factor of 4, but with smallest values over the city center. Consequently, the Bowen ratio exhibited even larger spatial variability, with a maximum value of about 1.8 over the city center and a minimum value of less than 0.2 over some nonurban areas. Spatial patterns of turbulent velocity variances are similar to those of the sensible heat flux. There are also large differences observed in average summertime heat fluxes in suburbs of North American cities located in different geographic regions (Grimmond and Oke, 1995).

The structure and dynamics of the daytime urban boundary layer are similar to the convective boundary layer over the surrounding rural area, except for the UBL being more turbulent, warm, dry, and polluted. The potential temperature profiles above the roof level are characterized by negative gradients in the shallow surface layer, very small (nearly zero) gradients in the much deeper urban mixed layer, and large positive gradients in the capping inversion layer. The urban heat-island intensity is relatively small in magnitude but extends through a significant portion of the mixed layer and up to tens of kilometers downwind of the city (Oke, 1995). Mean wind profiles also have large gradients in the surface layer including the urban canopy layer, relatively small gradients in the mixed layer, and much larger gradients in the capping inversion.

At night the urban boundary layer shrinks to a depth of a few hundred meters because strong stability of the approach flow suppresses turbulent mixing in the vertical direction. Still, the UBL over the city center is much thicker than the nocturnal stable boundary layer upwind of the city. The combination of increased temperatures (heat island) and increased roughness over a moderate-size and a large-size city can easily destroy the nocturnal surface inversion and dramatically modify the nocturnal boundary layer as it advects over the city. This process or phenomenon is illustrated in Figure 14.14, which shows a helicopter-measured along-wind vertical temperature cross-section, as well as the vertical potential temperature profiles at different locations in Montreal, Canada, on a winter morning. Other measurements of air temperature from automobile traverses in the city indicated an urban heat-island intensity of about 4.5 K at that time (Oke and East, 1971).

Figure 14.14 also shows that air is progressively warmed as it traverses the urban area (the weak flow from the N/NE was along the main helicopter traverse route), and the depth of the modified urban boundary layer increases downwind. At the rural site (sounding location 7) the atmosphere is very stable from the surface up to at least 600 m. In moving over the urban area, the bottom (urban canopy) layer becomes unstable and the layers above become neutral or weakly stable. Above the top of the UBL, the capping inversion layer retains the characteristics of the 'rural' approach flow. The UBL attains its maximum depth (300 m) over the city center and appears to become shallower farther downwind of the city center. A surface inversion may also reform over the downwind rural area. The newly developing rural boundary layer downwind of the city is, thus, a stably stratified internal boundary layer which grows slowly with distance. The modified urban air advecting above this shallow surface inversion layer is called the urban plume.

In comparison to the strong diurnal changes in stability of the lower atmosphere in surrounding rural areas, the urban atmosphere experiences only small diurnal variations in stability. The UBL remains well mixed both by day and by night, although the mixing depth usually undergoes a large diurnal oscillation.

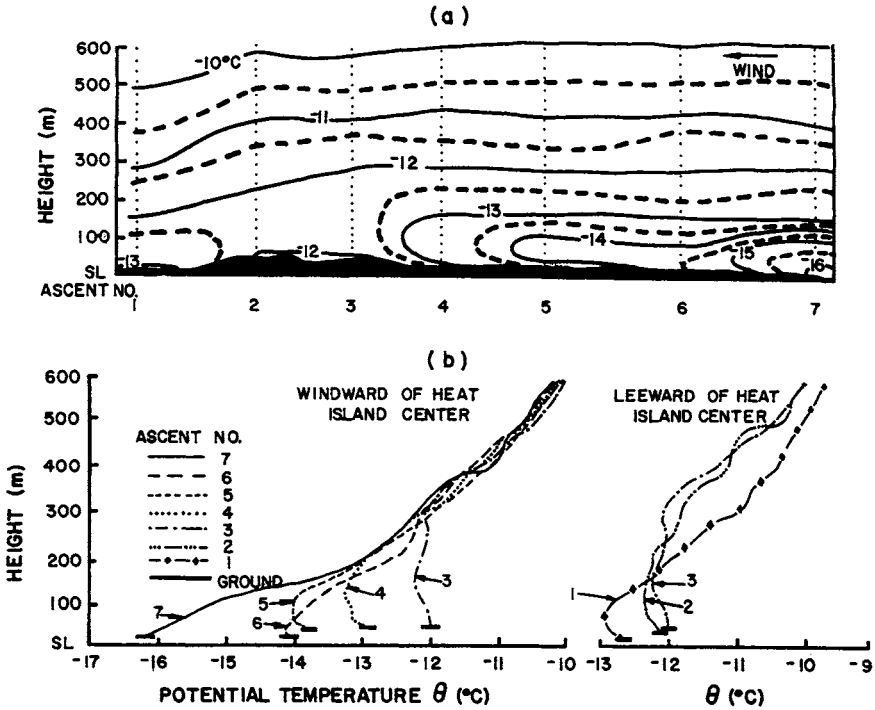

Figure 14.14 Modifications of potential temperature in the UBL due to the urban heat island over Montreal on a winter morning. (a) x-z cross-sectional distribution of Θ, and (b) vertical profiles of Θ at the various locations along wind. [After Oke and East (1971). Copyright © (1971) by D. Reidel Publishing Company. Reprinted by permission.]

The difference in the stabilities of the rural and urban boundary layers at nighttime explains why surface winds are often greater in the latter. Strong inversion reduces the near-surface winds in the rural area and essentially decouples them from stronger winds aloft. More efficient vertical mixing in the UBL, on the other hand, results in increased momentum (winds) in the surface layer.

Observational studies of the UBL have shown that the urban heat-island phenomenon, quantified by the urban–rural temperature difference, extends through the whole depth of the UBL. However, the heat-island intensity is maximum at the surface, decreases with height, and vanishes at the top of the UBL. There is also some evidence of the so-called cross-over effect, according to which the heat-island intensity becomes slightly negative above the top of the UBL (Oke and East, 1971; Oke, 1995). This effect is observed only at low wind speeds ($U < 3$ m s^{-1}).

A simple but appropriate relationship between the intensity of a nocturnal urban heat island and the maximum mixing depth over a city is

$$h_u = (\Theta_u - \Theta_r)/(\partial\Theta_r/\partial z) \cong (T_u - T_r)/[(\partial T_r/\partial z) + \Gamma] \qquad (14.13)$$

in which T_u and T_r are urban and rural air temperatures near the surface. It is based on the assumptions that the rural temperature sounding can be characterized by a constant gradient, at least above the shallow surface inversion layer, and there is no large-scale cold- or warm-air advection. Good agreement has been found between the predicted and observed values of h over New York, Montreal, and other cities. More sophisticated models will be needed to predict the growth of the UBL in approaching the city center from the edge of the city.

The urban heat island exerts strong influences on both the mean flow and turbulence structure of the UBL. The thermal anomaly represented by the city affects the approaching airflow by altering the local pressure field, by modifying the stability, and by increasing turbulence. The magnitudes of such influences depend upon the strengths of the gradient flow and the urban heat island (Oke, 1995).

With calm or very weak winds and a strong urban heat island, a thermally induced circulation system forms over the urban area and its rural environs. This circulation is essentially caused by the rising of warm air over the city and sinking of cold air over the surrounding countryside. The near-surface air from the rural surroundings converges toward the thermal low that forms over the city, while at the upper levels the airflow diverges away from the city. During the daytime, this circulation may extend up to the base of the lowest inversion, which may then acquire a dome shape with the maximum height near the city center. A radially symmetrical circulation would be expected to occur only over a circular city in the absence of gradient wind. More frequently, even light gradient winds over irregularly shaped urban heat islands cause more complex circulation patterns whose centers may not coincide with city centers. The low-level flow tends to accelerate toward the center of circulation and takes an anticyclonic curvature (Oke, 1995). Presence of topography and large green spaces (parks) in the urban area may also greatly influence these thermal circulations. Many observational, experimental, and numerical modeling studies of urban heat-island-induced circulations and urban boundary layers have been reported in the literature (Oke, 1987, 1995).

With stronger winds and therefore weaker urban heat island, the mechanical effects of increased surface roughness usually dominate over the thermal effects. Consequently, the mean wind speed decreases in going toward the city center. Even at a height of 100 m, the reduction in wind speed may be more than 20%. On the other hand, the surface drag or shear stress increases by more than 40%. Turbulence intensities are expected to increase even more, because σ_u, σ_v and σ_w

usually increase in proportion to u_* while mean wind speed decreases in going toward the city center. Wind direction shifts have also been observed in the near-surface air passing over the city. Wind first turns to the left or cyclonically in passing over the city and, then, to the right anticyclonically as the flow recovers its original direction downwind of the city. Wind direction shifts of 10–20° may occur over large urban areas. Such changes in the direction and magnitude of transport winds, as well as in turbulent intensities over and around urban areas have important consequences for the dispersion of pollutants from urban sources.

It has been commonly observed that the UBL is characterized by stronger turbulence as compared to the rural PBL upwind of the urban area. The increased turbulence is a result of the increased production of turbulence kinetic energy over an urban area due to increases in both the shear and buoyancy production terms in the TKE equation. Turbulent variances, fluxes and other statistics in the above canopy surface layer and the UBL, however, follow the same similarity scaling and display similar structure as turbulence in the homogeneous PBL for the same values of stability and other similarity parameters (Oke, 1995).

14.6 Building Wakes and Street Canyon Effects

In the preceding section we discussed the urban effects on the atmospheric boundary layer well above the urban canopy, and details of three-dimensional, complex flows around buildings were glossed over. For urban inhabitants, the local environment on streets around buildings, i.e., within the urban canopy, is perhaps more important than that in the above-canopy boundary layer. The canopy flow is much more complex, however, and is not amenable to any simple, generalized, quantitative treatment. Therefore, we give here only a brief qualitative description of some of the observed features of flow around buildings and other urban structures. These observations have largely come from physical simulations of flow around isolated and somewhat idealized buildings, as well as from clusters of buildings in environmental wind tunnels. Most of our conceptual understanding of such flows is derived from fundamental studies in bluff-body aerodynamics and environmental fluid mechanics.

14.6.1 Characteristic flow zones around an isolated building

There have been many experimental studies of flow distortion (modification) around isolated bluff bodies (e.g., circular and rectangular cylinders, flat plates, etc.) placed in a uniform, streamlined (laminar) approach flow. Comparatively

fewer studies have been made of the modified flow fields around surface-mounted structures immersed in thick boundary layers, as in the atmosphere. Although details of the modified flow vary with the characteristics of the approach flow, as well as with the size, shape, and orientation of the bluff body, certain flow phenomena and characteristic zones are commonly observed.

Flow separation and recirculating cavity Flow separation is said to occur when fluid initially moving parallel to a solid surface suddenly leaves the surface, because it can no longer follow the surface curvature or because of a break (discontinuity) in the surface slope. Flow separation is essentially a viscous flow phenomenon, as an inviscid or ideal fluid can, in principle, go around any bluff body without separation. The surface boundary layer developing in a real fluid flow, on the other hand, usually separates and moves out into the flow field as a free shear layer. The flow near the surface immediately downstream of the boundary layer separation is in the opposite direction. This is illustrated by the schematics of flow separation from a curved surface (Figure 14.15a) and a

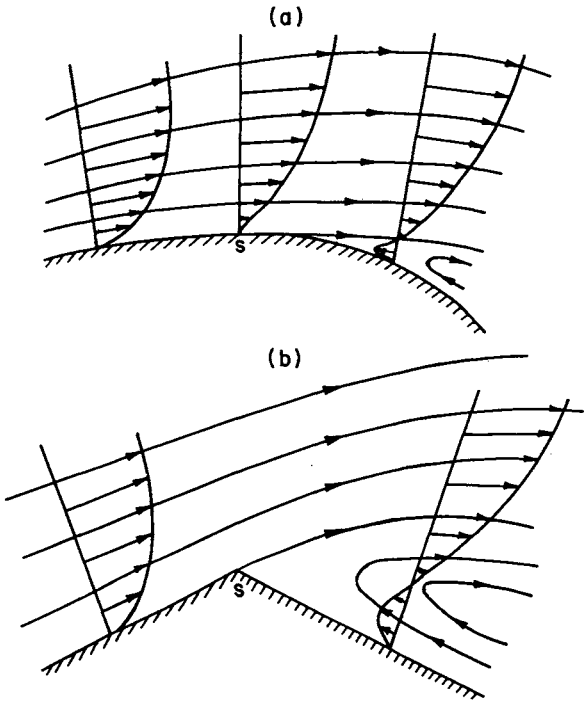

Figure 14.15 Schematic of flow separation from a (a) curved surface and (b) sharp-edged surface, and typical velocity profiles and streamline patterns.

sharp-edged surface (Figure 14.15b). Note that the surface streamline leaves off-tangentially or parallel to the initial slope from the separation point S.

The primary cause of flow separation is the loss of mean kinetic energy (e.g., in a diverging flow) in the boundary layer and consequent gain in the potential energy and, hence, in the surface pressure along the direction of flow, until the flow is no longer possible against the increasing adverse pressure gradient. All fluids have a natural tendency to flow in the direction of decreasing pressure, i.e., along a favorable pressure gradient. A significant adverse (positive) pressure gradient in the direction of flow can lead to abrupt and dramatic changes in the flow following its separation from the boundary.

The flow around a curved surface, as shown in Figure 14.15a, often leads to an unsteady separation in which the separation point S may not remain fixed but moves up and down the surface in response to perturbations to the flow, including the shedding of vortices by the separated shear layer. Even the average location of S is found to be quite sensitive to slight surface irregularities, as well as to the Reynolds number (Re), depending on the radius of curvature of the surface. On the other hand, the flow separation at a salient edge, as shown in Figure 14.15b, is steady, and its location is fixed, irrespective of the Reynolds number. This property is found to be quite useful in reduced-scale model simulations of atmospheric flows around buildings in fluid-modeling facilities, such as wind tunnels and water channels, in which Reynolds numbers are necessarily much smaller than those in the atmosphere. Gross features of flow around sharp-edged bluff bodies are found to be essentially Reynolds-number independent for all large enough Reynolds numbers (say, $\mathrm{Re} > 10^4$).

An example of flow separation from the upwind edge of the roof of a rectangular building is shown in Figure 14.16, in which other flow zones are also depicted. Note that the separated streamline eventually reattaches to the ground (or the roof in the case of a long building) at the downwind stagnation point. Below this a relatively stagnant zone of recirculating flow, or 'cavity,' is formed. Contaminants released into this region or those entrained from above often lead to very high concentrations in the cavity region, inspite of some cross-streamline diffusion and mixing with the outer fluid. The cavity region is characterized by a recirculating mean flow with low speeds but large wind shears and high-turbulence intensities. Flow separation also occurs from the sides of the building (not shown in Figure 14.16), so that the three-dimensional cavity is a complex structure.

Dimensions of the cavity envelope depend on the building aspect ratios W/H and L/H, where L, W, and H are the building length, width, and height, respectively, as well as on the characteristics of the approach flow, such as the boundary layer depth relative to the building height (h/H) and stability. In a neutral boundary layer, the maximum cavity length may vary from H (for $W/H < 1$) to $15H$ (for $W/H > 100$, and $L/H < 1$), while the maximum depth of

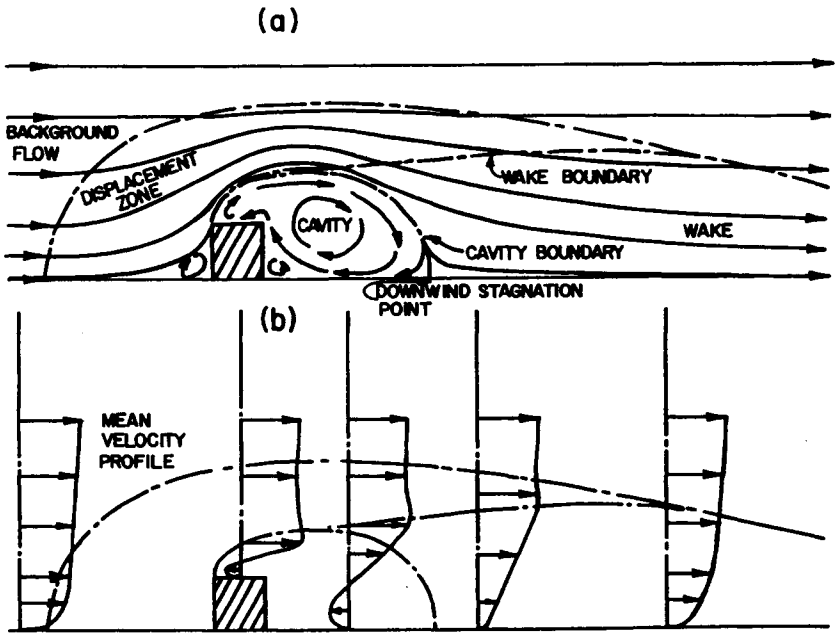

Figure 14.16 Schematic of displacement, cavity and wake flow zones around a two-dimensional sharp-edged building: (a) mean streamline pattern and (b) mean velocity profiles at the various locations along the flow. [After Halitski (1968).]

the cavity can vary between H and $2.5H$. For a more comprehensive review of wind tunnel and field data on cavity dimensions and empirical relations based on the same, the reader should refer to Hosker (1984).

Figure 14.16 also shows a small frontal cavity or vortex region confined to the upwind ground-level corner of the building. This is caused by the separation of the flow from the ground surface, resulting from an adverse pressure gradient immediately upwind of the building (note that the pressure is maximum at the stagnation point on the upwind face of the building).

Wake formation and relaxation The region of flow immediately surrounding and following the main recirculating cavity, but still affected by the building, is called the building 'wake.' According to some broader definitions, the wake also includes the lee-side cavity region, sometimes called the 'wake cavity,' and comprises the entire downstream region of the flow affected by the obstructing body (all bluff and streamline bodies have wakes, even though some may not have any recirculating cavity in their lee). Here we use the more restrictive definition excluding the cavity from the wake, so that there is no flow reversal in the latter.

Sometimes the wake is subdivided into the 'near wake' and the 'far wake.' The mean flow and turbulence structure in the former are strongly affected by separating shear layers, as well as by vortices shed from the building edges, as shown in Figure 14.17. The separated shear layers have large amounts of vorticity, generated when these layers were still attached to the building as a boundary layer. They also have strong wind shears across them. After separation the shear layers become unstable and generate a lot of turbulence and, frequently, also periodic vortices called Karman vortices, which grow as they travel downwind. Another prominent vortex system in flows around three-dimensional surface obstacles is the so-called horseshoe vortex. It is a standing horizontally oriented vortex generated near the ground upwind of the obstacle; it wraps around the obstacle and then trails off downwind as a counter-rotating vortex pair (Figure 14.17). This vortex resembles a horseshoe when viewed from above, hence its name. These large vortices produce oscillations in the wake boundary, while smaller eddies transport momentum across mean streamlines. As a consequence of these processes, mean velocity in the direction of flow decreases rapidly, while turbulence increases with downwind distance in the near wake, which may extend up to a few building heights from the upwind face of the building. Building-generated turbulence is found to be predominant in the near wake and cavity regions.

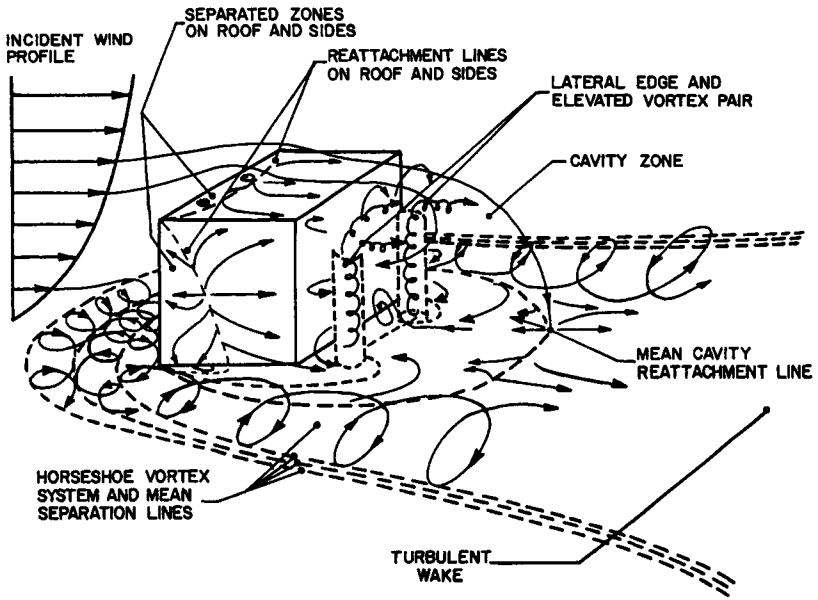

Figure 14.17 Schematic of separated flow zones and vortex systems around a three-dimensional sharp-edged building in a deep boundary layer. [After Woo *et al.* (1977).]

The near wake is followed by a more extensive far-wake region in which perturbations to mean flow and turbulence decay with distance, following an exponential or power law, and become insignificant only at large downwind distances. The longitudinal, lateral, and vertical extents of the wake depend on building dimensions and their aspect ratios. Both the width and the thickness (height) of the wake grow with distance behind the building, if the wake is defined as the region encompassing all building-induced perturbations to the background or approach flow, even if they become practically undetectable. This is the classical theoretical definition of wake, which extends to infinity along the flow direction as it grows in cross-wind directions. A more practical definition of the wake in which perturbations in the mean and turbulent flow are significant and measurable, i.e., they are larger than a certain specified percentage (say, 10%) of the background flow, would make the wake boundary a finite envelope with a maximum length, width, and height, which depend on building aspect ratios. Wind tunnel observations in simulated building wakes indicate that significant building-induced perturbations to flow may not extend beyond 10 to 20 building heights in the downwind direction and 2 to 3 building heights or widths in other directions. Sometimes, the far wake is further subdivided into an inner layer or a surface layer, and an outer mixing layer. The former is assumed developing downwind of the cavity reattachment point and has the character of an internal boundary layer in which flow adjusts to the local surface (see Plate, 1971, Chapter 4). The outer mixing layer has the character of a classical wake far from any bounding surface.

External region of streamline displacement A third region of relatively minor modifications to the flow also envelops the building and its wake and cavity regions. Streamlines in this so-called external or displacement region are at first deflected upward and laterally outside in response to the growing wake, and then downward and inside to their undisturbed pattern, as the building influence decays and disappears. These displacements and associated perturbations to the flow decrease with increasing distance outward from the wake boundary. Such perturbations to the flow in the external region are considered to be essentially inviscid and small, allowing for simplified theoretical treatments. Note that external zones of streamline displacement must also exist, to some extent, in all the nonhomogeneous boundary layers (Townsend, 1965). Outside the displacement zone is the region of undisturbed flow.

14.6.2 Clustering and street canyon effects

In urban settings, buildings are placed in clusters of individual houses, high-rise apartments, or commercial buildings. When the spacing between adjacent

buildings is less than 10 to 20 building heights, which is generally the case, the wakes and cavities associated with individual buildings interact, producing a variety of complicated and often discomforting flow patterns. There have been only a few simulation studies of clustering effects of buildings in urban settings, and one or two field studies (Hosker, 1984). Theory and numerical simulations cannot cope with such complex and highly turbulent flows. Experimental efforts are also beset by serious instrumental and logistical difficulties. Our qualitative understanding of flow phenomena associated with building clusters is largely due to wind tunnel simulation studies (Jeram *et al.*, 1995).

When buildings are nearly of the same size and height, and are arranged in regular rows and columns parallel to straight streets in an otherwise flat area, air flow is accelerated just above the roof level outside of any roof cavities, as well as in any side streets parallel to the wind direction. Winds can become strong and steady, particularly in narrow and deep street canyons, due to direct blocking of flow by windward faces of the buildings and channeling in side-street canyons. Streets normal to the ambient wind direction are relatively sheltered when the ambient atmospheric boundary layer flow is weak, but strong standing vortices can develop in cross-streets at moderate ambient wind speeds. These are augmented forms of lee-side cavities where the recirculating flow is enhanced by deflection down the windward face of the adjacent downstream building. Winds are more gusty (turbulent) in the presence of these building-induced vortices. If the ambient wind flow is at an angle to the streets or buildings, lee-side vortices take on a 'corkscrew' motion with some along-street movement. The winds in the side streets are also reduced and become more gusty, reflecting intensification of corner vortices. All of the above-mentioned flow patterns strongly depend on building aspect ratios and the relative spacing between them. Irregular arrangements of building blocks along curved streets can result in an almost infinite variety of flow patterns. Some of the basic fluid flow phenomena underlying these complex flow patterns are schematically illustrated and discussed by Hosker (1984).

When adjacent buildings in a cluster differ considerably in their heights or aspect ratios, flow patterns around them become even more complex and highly asymmetrical. Although a wide variety of situations can be visualized and actually occur in urban settings, systematic experimental studies (primarily wind tunnel simulations) are so far confined to the so-called two-body problem in which a much taller building is placed downwind of a shorter building, or vice versa (Hosker, 1984). Here, too, the flow patterns depend strongly on the relative building heights, spacing between the two buildings, and the building aspect ratios, as well as on the characteristics of the approach flow. The presence of a much smaller building upwind of a tall building appears to affect only the upwind portion of the horseshoe vortex, which wraps around any isolated building, and the downwind cavity and wake of the taller building are less

affected. These can be considerably modified, however, if the shorter building is placed downstream of the taller buildings. The taller building has a more dominating influence on the circulation around a smaller building in its wake than the other way around.

14.7 Other Topographical Effects

In this section we consider the effects of small hills, ridges, and escarpments on atmospheric boundary layer flows. Effects of large mountains extend well above the boundary layer and involve mesoscale and, sometimes, synoptic-scale motions, which are outside the scope of this book. Unlike the flows around sharp-edged buildings or groups of buildings in which mechanically generated turbulence dominates over the ambient turbulence in the approach flow, flows around gentle, low hills and ridges are quite sensitive to mean shear, stratification, and turbulence in the approach flow. Therefore, their description is presented here according to different approach flow conditions. This is largely based on laboratory fluid-modeling experiments, some theoretical and numerical model studies, and a few field experiments. For more comprehensive reviews of the literature, the reader should refer to Hunt and Simpson (1982), Taylor *et al.* (1987), and Bains (1995).

14.7.1 Neutral boundary layer approach flow

The characteristic flow zones shown in Figure 14.16 for the boundary layer modified by an isolated building can also be applied to neutral boundary layer flow around an isolated hill, ridge, or escarpment. However, flow separation and associated cavity regions are likely to be unsteady and much smaller, if they exist at all, around gentle topographical features. The flow may not separate even on the lee side, unless the maximum downwind slope is large enough (say, ≥ 0.2). Behind long, steep ridges, however, the cavity region may extend up to 10 hill heights in the downstream direction. The cavity is at most a few hill heights long and frequently smaller for thee-dimensional hills.

An important universal feature of the flow over a hill is its speeding up in going over the hill's top. For quantifying this, a speed-up factor $S_F = U(z)/U_0(z)$ is defined as the ratio of wind speed at some height above the hill to that at the same height above the flat surface in the approach flow. While S_F decreases with increasing height, its maximum values range from just over 1 to about 3, depending on the hill slope, and aspect ratio. The largest speed-up factors are observed over three-dimensional hills of moderate slope. In approaching an isolated hill or a two-dimensional ridge, the flow near the surface first

decelerates slightly before reaching the upwind base of the hill and then accelerates in going over the hill. Flow also accelerates in going around the hillsides. These features, as well as deceleration in the near wake, are shown in Figure 14.18, based on measurements over an approximately circular hill (Brent Knoll).

Another feature of the air flow over a hilltop is that the wind speed increases with height much more rapidly than it does over a level ground. Above this shallow surface shear layer, the wind profile becomes nearly uniform; sometimes it is characterized by a maximum wind speed (low-level jet) near the surface. Wind profiles at the tops of escarpments are also found to have similar characteristics.

The lee-side hill wakes are similar to building wakes; these are characterized by reduced mean flow and enhanced turbulence. The maximum topographically induced perturbations to the flow in the near wake depend on the aspect ratio, slope, and shape of the hill. However, their decay with distance in the far wake appears to follow similar relations. In particular, the maximum velocity deficit $(\Delta U)_{\max}$ is given by

$$(\Delta U)_{\max}/U_0 = m(x/H)^{-1} \tag{14.14}$$

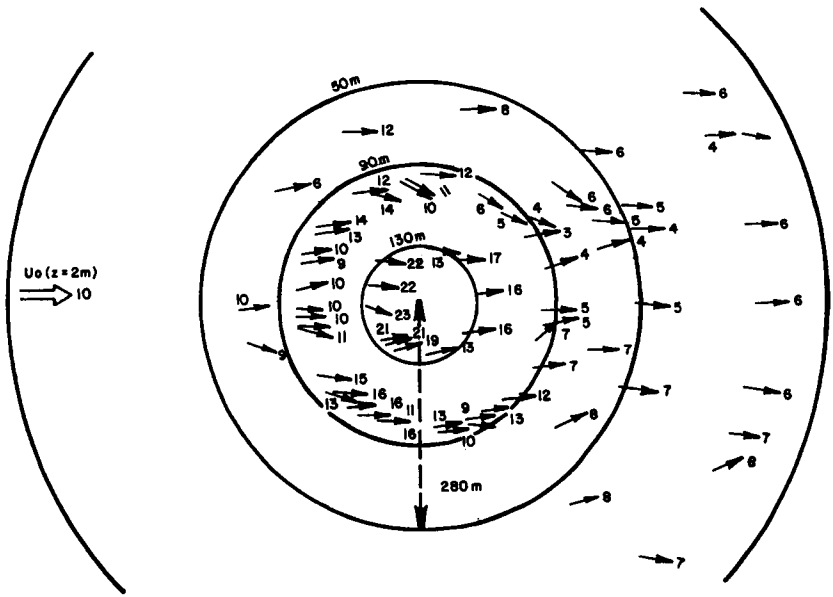

Figure 14.18 Observed mean wind speeds and directions near the surface (z = 2 m) of an approximately circular low hill (Brent Knoll). [After Mason and Sykes (1979).]

where U_0 is the mean velocity at hill height in the approach flow, and m is a coefficient depending on the hill and boundary layer parameters. The rate of growth of the wake also depends on the hill slope and aspect ratio (Arya *et al.*, 1987).

Flow at an oblique angle to a long ridge is often characterized by the generation of trailing vortices and a persistent swirling turbulent flow in the wake. Thus, the ridge acts like a vortex generator. These and other three-dimensional effects of hills are poorly understood, and so are the Coriolis effects of the earth's rotation on flow around hills.

Very few systematic studies have been made on groups of hills and valleys. The simplest arrangement is that of similar, nearly two-dimensional ridges and valleys located parallel to each other. Wind tunnel experiments indicate that the speed-up of flow over the ridge top and the flow distortion in the near wake are maximum for the first ridge and valley, as if downwind ridges did not exist. But these effects diminish in the downwind direction as subsequent ridges and valley interact with the flow. After the first few ridges and valleys, the speed-up factor over the tops of ridges approaches a constant value of only slightly above unity, and the summit velocity profile assumes a new logarithmic form with nearly the same roughness length as upwind. Turbulence intensities over the hill crests do not differ much from their undisturbed (flat terrain) values except for some enhancement of the lateral component σ_v/U for wind directions not normal to ridges and valleys. In the valleys between the ridges mean flow is reduced, with possible recirculation cavities forming over steeper lee-side slopes, and turbulence is considerably enhanced. These results have been confirmed in a recent field study of atmospheric flow over a succession of ridges and valleys under near-neutral conditions (Mason and King, 1984). When the flow is across the valley, wind speeds in the valley are about one- to two-tenths of that on the summit. The size of the separated region is very sensitive to flow direction and the presence of any sharp discontinuity in the terrain profile. When the flow is predominantly along the valley, wind speeds in the valley are higher, but still less than that on the summit, and no channeling effect is observed, at least in near-neutral conditions.

A grouping of three-dimensional hills can produce complex flow patterns, similar to those for groups of buildings. For example, channeling of flow between two round hills or in a gap between a long ridge often leads to strong, persistent winds. These effects are particularly pronounced in the presence of stable stratification, which forces the flow to go around rather than over the hills.

14.7.2 Stably stratified approach flow

Effects of topography on the flow are considerably modified in the presence of stable stratification. Some of the effects and the associated flow patterns are

qualitatively similar to those for the neutral flow, although stratification does influence their intensity. Other effects are peculiar to stably stratified flows over and around hills, e.g., the generation of lee waves, formation of rotors and hydraulic jump, inability of the low-level fluid to go over the hills, and upstream blocking.

Stratification effects on flow around topography are generally described in terms of a Froude number (F or F_L) based on the characteristic height (H) or length scale (L_1) of the topographical feature in the direction of flow

$$F = U_0/NH \tag{14.15}$$

$$F_L = U_0/NL_1 \tag{14.16}$$

Where U_0 is the characteristic velocity of approach flow (say, at $z = H$), and N is the Brunt–Baisala frequency

$$N \equiv \left(-\frac{g}{\rho_0}\frac{\partial \rho}{\partial z}\right)^{1/2} = \left(\frac{g}{\Theta_0}\frac{\partial \Theta}{\partial z}\right)^{1/2} \tag{14.17}$$

which is the natural frequency of internal gravity waves or lee waves; the corresponding wavelength is $\lambda = U_0/2\pi N$. Physically, the Froude number is the ratio of inertia to gravity forces determining the flow over topography. It has an inverse-square relationship to the bulk Richardson number, i.e., $F \sim \mathrm{Ri}_B^{-2}$. Note that if $F \ll 1$ the stratification is considered to be strong, while for $F \gg 1$ it is near neutral ($F = \infty$ for a strictly neutral stability). The Froude number also provides the criteria for the possible generation of lee waves and separation of flow in the lee of the hill. In particular, simple Froude number criteria have been developed from theory and experiments in the simple case of a uniform, inviscid approach flow with constant density or potential temperature gradient (Hunt and Simpson, 1982; Bains, 1995). These are schematically shown in Figure 14.19 for two-dimensional hills. Here, the critical Froude number (F_c) for separation represents the highest value of F at which the boundary layer separation is suppressed by lee waves. It depends on the stratification of the approach flow, as well as on the various hill parameters (e.g., height, aspect ratio, and shape).

Figure 14.19 also indicates that different types of flow patterns may develop in the lee of a two-dimensional hill, depending on the Froude number and the maximum hill slope. Similar and other types of flow phenomena are found to occur in the lee of three-dimensional hills and under different approach flow conditions (e.g., stratified shear flow and mixed layer capped by an elevated inversion). Perhaps the most spectacular flow phenomena related to topography are the severe downslope winds, locally known as Chinook, Föhn, or Bora, followed by a 'hydraulic jump.' These are analogous to the passage of water

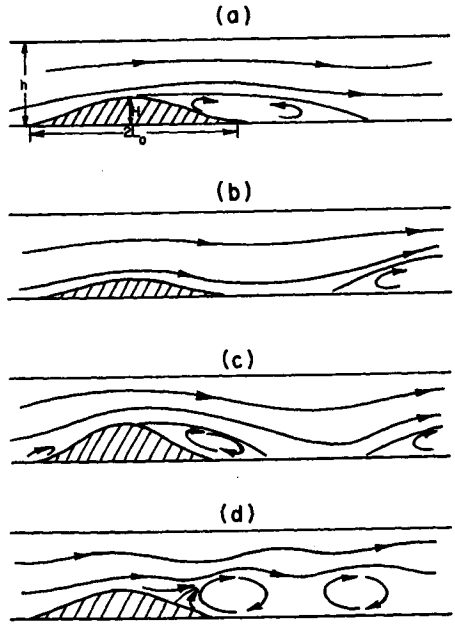

Figure 14.19 Stratified flows over two-dimensional hills in a channel or under a strong inversion, showing the effect of lee waves on flow separation. (a) Supercritical $F > F_c$, no waves possible; separation is boundary-layer controlled. (b) Hill with low slope; subcritical $F < F_c$, downstream separation caused by lee-wave rotor. (c) Hill with moderate slope; supercritical $F > F_c$, boundary-layer separation on lee slope. (d) Hill with moderate slope; subcritical $F < F_c$, lee-wave-induced separation on lee slope. [After Hunt and Simpson (1982).]

over a dam spillway as it is rushing down at very high speeds and creating a violent hydraulic jump at the base of the dam. The necessary approach flow conditions for the corresponding atmospheric flow are a strong, elevated inversion capping a high-speed mixed-layer flow of depth $h > H$, such that $U_0/N(h - H) \cong 1$, where N is the Brunt–Vaisala frequency for the inversion layer. Figure 14.20 shows the schematics of two widely different, but possible, flow patterns with an approach mixed-layer flow. Note that, here, the relevant Froude number determining the flow over the hill is $U_0/N(h - H)$.

An important aspect of stably stratified flows over and around three-dimensional topographical features is the increasing tendency of fluid parcels to go around rather than over the topography with increased stratification (decreasing Froude number). This is because such fluid parcels do not possess sufficient kinetic energy to overcome the potential energy required for lifting the parcel through a strong, stable density gradient. Whether a given parcel in the

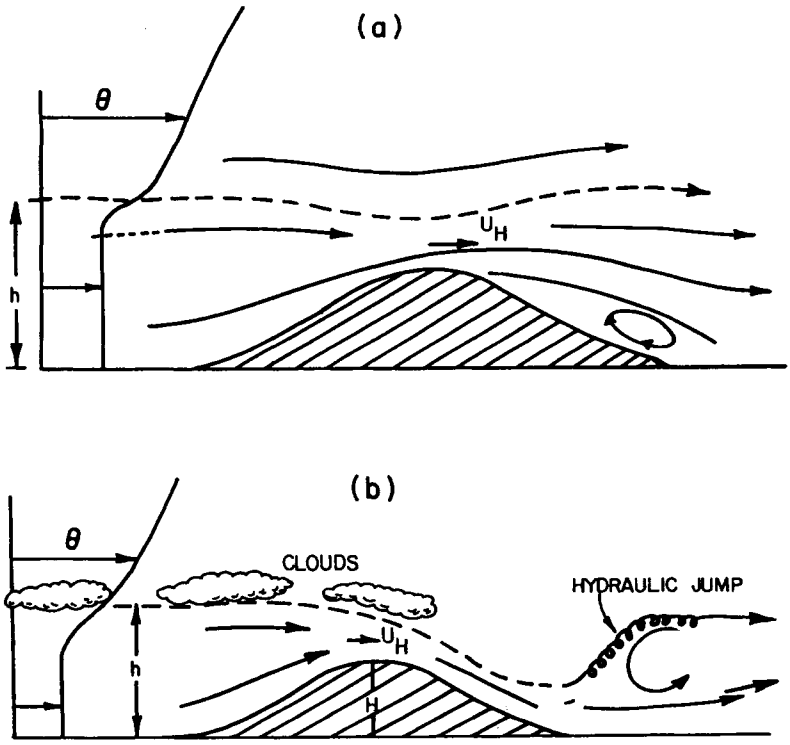

Figure 14.20 Schematics of air flow over a two-dimensional ridge with an elevated inversion upwind. (a) Low wind speed with $U_0/N(h - H) \ll 1$, flow separation on lee slope. (b) High wind speed with $U_0/N(h - H) \cong 1$, no flow separation on lee slope, hydraulic jump downwind. [After Hunt and Simpson (1982).]

approach flow would go over or around the hill depends on the height of the parcel relative to hill height, its initial lateral displacement from the central (stagnation) streamline, shear and stratification in the approach flow, and topographical parameters. Parcels approaching the hill at low heights are likely to go around, while those near the hilltop may go over the hill. One can define a dividing streamline that separates the flow passing around the sides of the hill from that passing over the hill. The height H_s of this dividing streamline can be estimated from the simple criterion that the kinetic energy of a fluid parcel following this streamline be equal to the potential energy associated with stratification that the parcel must overcome, i.e.,

$$\tfrac{1}{2}\rho U_0^2 = g\int_{H_s}^{H}(H - z)\left(-\frac{\partial\rho}{\partial z}\right)dz \tag{14.18}$$

where U_0 is the approach flow velocity at $z = H_s$. This integral equation, first suggested by Sheppard (1956), can be used for any approach flow and topographical arrangement. In practice, it must be solved for H_s iteratively, because the unknown appears as the lower limit of integration. For the particular case of a stratified approach flow with a constant density gradient, Equation (14.18) reduces to the simpler formula

$$H_s = H(1 - F) \tag{14.19}$$

which was suggested by Hunt and Snyder (1980) on other theoretical and experimental bases.

Laboratory experiments and a few observations of smoke plumes impinging on hillsides have confirmed the validity and usefulness of the dividing streamline concept (Snyder *et al.*, 1985). These also indicate that Equation (14.18) provides only a necessary (but not the sufficient) condition for the fluid above H_s to go over rather than around a hill. It can still pass around the sides and take a path requiring less potential energy to overcome than that given by Equation (14.18). Experiments also indicate that the lateral aspect ratio (W/H) of the hill is relatively unimportant, but the stratification and shear in the approach flow, upwind slope of the hill, and obliqueness of the flow to an elongated hill are all important in determining the flow over and around the hill (Bains, 1995).

In the case of strongly stratified ($F \ll 1$) flow approaching normal to a very long (nearly two-dimensional) ridge, there is a distinct possibility of upstream blocking of the fluid, because very little can go over the ridge. A region of nearly stagnant fluid occurs below the dividing streamline and far away from the edges where it can go around the ridge. Such a flow field may not acquire a steady state, because the upwind edge of the blocked flow propagates farther upstream as a density front and certain columnar disturbance modes and gravity waves generated near the ridge can also propagate upstream. Topographically blocked flows have important implications for local weather and for dispersion of pollutants from upwind sources.

In stably stratified flows over hills and mountain ridges, a variety of flow patterns may develop on the lee side, depending on the Froude number, hill slope and shape, presence of elevated inversions, and wind shear (Hunt and Simpson, 1982; Bains, 1995). Perhaps, the most spectacular of these are strong downslope winds as gravity flows, which are sometimes followed by a hydraulic jump. Similar phenomena have also been observed in laboratory experiments on stratified water flows over model hills (Bains, 1995). Cold downslope winds, called bora, have been observed in different parts of the world, but most notably along the coast of Yugoslavia (Atkinson, 1981, Chapter 3). Some of the boras start rather abruptly, while others develop gradually over several hours as the

synoptic flow pattern changes to the appropriate direction (normal to the mountain ridge).

Strong downslope winds also occur when warm and moist winds are forced up the slope of a tall mountain ridge resulting in condensation and precipitation near the top of the mountain. With most of the moisture removed from the air and the latent heat of condensation added to the same, the drier and warmer air begins to descend on the lee side slope, where it becomes much warmer due to dry adiabatic compression. Such orographically forced warm and dry downslope winds have acquired local names such as chinook, foen, and Santa Anna, depending on their geographical location. Both cold and warm downslope winds are strong, gusty, dry and fairly constant in direction. The approach flows typically associated with these winds are normal to the mountain ridges and usually contain a stable layer at a critical height (Atkinson, 1981, Chapter 3).

When the approach flow is stably stratified, any lee-side separation of flow may be suppressed by stratification. But it can be induced by lee waves and their associated rotors under appropriate conditions (Hunt and Simpson, 1982). Since the flow is usually separated from the hillsides, the near-wake region is always turbulent even when the approach flow may not be turbulent, especially outside of the shallower stable boundary layer. This has important implications for the dispersion of pollutants at nighttime from sources near the downwind base of a hill.

Vortex streets are often shed by hill sides, especially under strongly stratified flows with a low-level inversion. Satellite photographs of vortex streets downwind of small, isolated mountain islands show their wakes extending up to several hundred kilometers (Atkinson, 1981, Chapter 4). Experimental and theoretical studies of obstacle wakes in stably stratified flows have been reviewed by Bains (1995). Most of these studies considered only uniform, laminar, linearly stratified flows over or around idealized two- or three-dimensional hills. For a given hill shape and size, wake phenomena are described primarily as a function of Froude number or Richardson number. The effects of wind shear, large surface roughness, and complex irregular topography, such as those commonly encountered in nature, are hardly understood. A few field studies of near-surface flow around small, isolated hills and ridges have been conducted, but measurements did not extend into the far-wake region.

Example Problem 2

A uniform stably stratified flow with a characteristic velocity of $10\ \mathrm{m\ s^{-1}}$ outside the shallow stable boundary layer of depth $h = 100$ m and temperature gradient of $0.02\ \mathrm{K\ m^{-1}}$ approaches an isolated hill of height $H = 400$ m. The characteristic surface air temperature is 12°C and the surface pressure is about 1000 mb at the upwind base of the hill.

(a) Calculate the Brunt–Vaisala frequency and the characteristic wavelength of the lee waves that might be produced in the lee of the hill.
(b) Estimate the height of the dividing streamline below which the air flow might be expected to go around rather than over the hill.

Solution

(a) The Brunt–Vaisala frequency is given by

$$N = \left(\frac{g}{\Theta_0}\frac{\partial \Theta}{\partial z}\right)^{1/2}$$

in which,

$$\Theta_0 = 273.2 + 12 = 285.2 \text{ K}$$

$$\frac{\partial \Theta}{\partial z} = \frac{\partial T}{\partial z} + \Gamma = 0.02 + 0.0098 \cong 0.03 \text{ K m}^{-1}$$

Thus,

$$N = \left(\frac{9.81}{285.2} \times 0.03\right)^{1/2} \cong 0.0321 \text{ Hz}$$

The characteristic wavelength of hill-induced lee waves is given by

$$\lambda = \frac{U_0}{2\pi N} = \frac{10}{2\pi \times 0.0321} \cong 49.6 \text{ m}$$

(b) The height of dividing streamline is given by Equation (14.19)

$$H_s = H(1 - F)$$

where F is the Froude number based on the hill height, i.e.,

$$F = \frac{U_0}{NH} = \frac{10}{0.0321 \times 400} \cong 0.78$$

so that,

$$H_s = 400(1 - 0.78) \cong 88 \text{ m}$$

Thus, the shallow stable boundary layer flow below the height of 88 m is expected to go around the hill.

14.8 Applications

Spatial variations of surface roughness, temperature, wetness, and elevation frequently cause nonhomogeneous atmospheric boundary layers developing over these surface inhomogeneities. A basic understanding of horizontal and vertical variations of mean flow, thermodynamic variables, and turbulent exchanges in nonhomogeneous boundary layers is essential in micrometeorology and its applications in other disciplines and human activities. Specifically, the following applications may be listed for the material covered in this chapter.

- Determining the development of modified internal boundary layers following step changes in surface roughness and temperature.
- Determining the fetch required for air flow adjustment to the new surface following a discontinuity in surface elevation or other properties.
- Selecting an appropriate site and height for locating meteorological or micrometeorological instruments for representative observations for the local terrain.
- Determining wind and air mass modifications under situations of cold or warm air advection over a warmer or colder surface.
- Estimating urban influences on surface energy balance and surface and air temperatures.
- Determining possible modifications of mean flow, turbulence, and the PBL height over an urban area.
- Estimating transport and diffusion of pollutants in the urban boundary layer and the urban plume.
- Estimating pollutant dispersion around hills and buildings.
- Estimating wind loads on buildings and knowing the wind environment around buildings.
- Siting and designing wind-power generators in hilly terrain.
- Other wind-engineering applications in urban architecture and planning.

Problems and Exercises

1. A near-neutral atmospheric boundary layer 1500 m thick encounters a sudden change in the surface roughness in going from land ($z_0 = 0.1$ m) to a large lake ($z_0 = 0.0001$ m) of the same surface temperature. The observed wind speed at 10 m height in the approach flow is 10 m s^{-1}. Assuming that the overall PBL thickness ($h = 1500$ m) and the surface layer thickness ($h_s \cong 150$ m) remain unchanged over the lake, calculate and plot the following parameters, using Equations (14.1) and (14.3), with $a_i = 0.4$ for the internal boundary layer.

(a) The IBL height as a function of distance, and the distances where it reaches the top of the approach flow surface layer and the PBL.
(b) The friction velocity and wind speed at 10 m height over the lake as functions of distance from the shore.

2. Repeat the calculations in Problem 1 for the case of an onshore neutral boundary layer flow with the same wind speed (10 m s^{-1}) and depth (1500 m) over the lake, and compare the results for the two cases.

3. Calculate and graphically compare the development of thermal internal boundary layers in the following two situations, using appropriate expression for h_i:
(a) A stably stratified boundary layer flow with $\partial\Theta/\partial z = 0.02$ K m^{-1} over land advecting over a 15°C warmer sea.
(b) An unstable warm continental boundary layer with a lapse rate of 0.02 K m^{-1} advecting over a 15°C colder sea surface. Assume a typical drag coefficient of 0.9×10^{-3} for the stably stratified IBL.

4.
(a) What are the leading causes and mechanisms for the formation of an urban heat island?
(b) If the population of a midwestern United States city has increased from 100 000 to 1 000 000 in the past 20 years, estimate the expected change in its maximum heat-island intensity and the annual rate of urban warming over that period.

5.
(a) Give physical reasons for the urban mixed-layer dome phenomenon and list conditions under which it might be enhanced and those in which it would be suppressed.
(b) Calculate and compare the nocturnal urban mixed-layer height at the city center, where the near-surface temperature is 15°C, with that at a suburban location of near-surface temperature 12°C, when the upwind rural sounding indicates a temperature gradient of 0.02°C m^{-1} over a deep-surface inversion layer and a near-surface temperature of 9°C.

6.
(a) What are the causes and consequences of boundary layer separation from hills and buildings?
(b) In what respects do the cavity and near-wake flow regions behind an isolated square-shaped building differ from those behind a cylindrical building?

7.

(a) Why is the length of a recirculating cavity region behind a long ridge much larger than that behind an axisymmetrical hill of the same height and slope?

(b) In what respects does a three-dimensional hill wake differ from a building wake?

8.

(a) Show that, for constant density-gradient uniform or shear flow, Equation (14.18) reduces to Equation (14.19).

(b) Calculate the dividing streamline height for a constant gradient shear flow with $\partial U_0/\partial z = 0.1\ \mathrm{s}^{-1}$, $\partial\Theta/\partial z = 0.05\ \mathrm{K\ m}^{-1}$, and $\Theta_0 = 280\ \mathrm{K}$, approaching an axisymmetric hill 200 m high. What are the implications of this to flow over and around the hill?